Influence of the Retinal Blood Vessel Topography on the Variability of the Retinal Nerve Fiber Bundle Trajectories in the Human Retina

Kunliang Qiu,[1,2] Julia Schiefer,[3] Jukka Nevalainen,[4] Ulrich Schiefer,[5,6] and Nomdo M. Jansonius[1,7]

[1]Department of Ophthalmology, University of Groningen, University Medical Center Groningen, Groningen, The Netherlands
[2]Joint Shantou International Eye Center of Shantou University and The Chinese University of Hong Kong, Shantou, Guangdong Province, People's Republic of China
[3]University Eye Hospital Munich, Ludwig Maximilians University, Munich, Germany
[4]University Eye Hospital Oulu, Oulu, Finland
[5]Centre for Ophthalmology, University of Tübingen, Tübingen, Germany
[6]Competence Center "Vision Research," University of Applied Sciences, Aalen, Germany
[7]Department of Epidemiology, Erasmus Medical Center, Rotterdam, The Netherlands

Correspondence: Nomdo M. Jansonius, Department of Ophthalmology, University Medical Center Groningen, PO Box 30.001, 9700 RB Groningen, The Netherlands; n.m.jansonius@umcg.nl.

Submitted: June 9, 2015
Accepted: August 13, 2015

Citation: Qiu K, Schiefer J, Nevalainen J, Schiefer U, Jansonius NM. Influence of the retinal blood vessel topography on the variability of the retinal nerve fiber bundle trajectories in the human retina. *Invest Ophthalmol Vis Sci*. 2015;56:6320–6325. DOI:10.1167/iovs.15-17450

Purpose. To determine the relationship between the retinal blood vessel topography and the retinal nerve fiber bundle (RNFB) trajectories in the human retina.

Methods. A previously collected dataset comprising 28 fundus photographs with traced RNFB trajectories was used. For all traced trajectories, the departure from our previously published RNFB trajectory model was calculated. Subsequently, we calculated, per subject, a "mean departure" for the superior-temporal and inferior-temporal region. We measured angles between a line connecting the optic nerve head (ONH) center and the fovea and lines connecting the ONH center and the crossings of the superior and inferior temporal arteries (arterial angles) and veins (venous angles) with circles around the ONH; circle radii were 25%, 50%, and 100% of the ONH center-to-fovea distance. We also defined two angles based on the location of the first arteriovenous crossing. Multiple linear regression analysis was performed with mean departure as dependent variable and refraction, ONH inclination, and vessel angles as independent variables.

Results. In the superior-temporal region, refraction ($P = 0.017$), ONH inclination ($P = 0.021$), and the arterial angle corresponding to the middle circle ($P < 0.001$) were significant determinants of mean departure. Explained variance was 0.54. In the inferior-temporal region, the arterial angle corresponding to the largest circle ($P = 0.002$) was significant. Explained variance was 0.32.

Conclusions. The retinal blood vessel topography explains a significant part of the RNFB trajectory variability but only if (1) the vessel topography is assessed at an appropriate distance from the ONH and (2) the superior and inferior hemifield are addressed independently.

Keywords: retinal nerve fiber layer, retinal vessels, retinal vasculature

Glaucoma is one of the important causes of blindness, with irreversible damage to retinal ganglion cells, the retinal nerve fiber layer (RNFL), and the optic nerve as its pathological features. The detection of changes in these structures is part of the diagnostic armamentarium in glaucoma; a detailed anatomical knowledge of especially the retinal nerve fiber bundle (RNFB) trajectories is helpful to integrate information from each structure and to topographically correlate it with visual field data.

In 2000, Garway-Heath et al.[1] reported nerve fiber bundle trajectories based on fundus photographs. Later, models based on axonal growth and maps based on the correspondence between optical coherence tomography thickness measurements and visual field data were published.[2–5] We developed a mathematical model describing the RNFB trajectories with their intersubject variability, based on fundus photographs.[6,7] A considerable variability was found, confirming the earlier findings.[1] Recently, computational models mapping visual field locations to optic nerve head sectors were reported.[8,9]

The influence of anatomical variables including refraction, axial length, optic disc position, and optic disc dimensions on the RNFB trajectories has been studied as well.[7,8,10] Although significant factors were identified, the sources of the variability of the RNFB trajectories are not fully understood.

It has been reported that the vascular and neuronal systems share many similarities. The blood vessels and nerves tend to develop in relative proximity, throughout the body of any species in general and in the primate retina in particular.[11,12] In the primate (human and macaque) retina, the vessels grow along the retinal ganglion cell layer/RNFL interface, except for the vessels in the vicinity of the fovea.[12] By using scanning laser polarimetry, Resch et al.[13] reported that the peripapillary

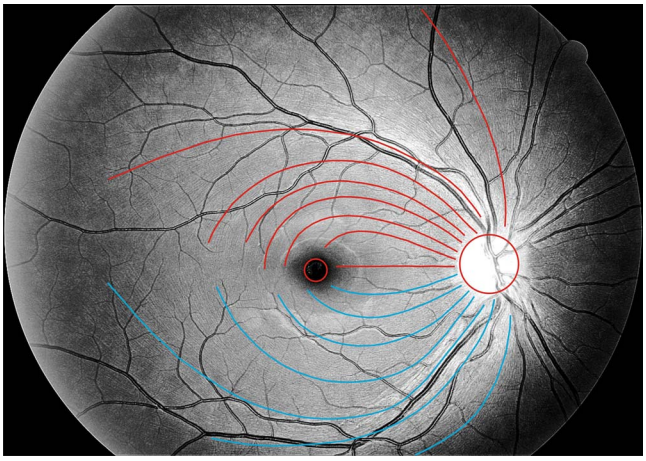

FIGURE 1. Example of a fundus photograph with traced trajectories. *Colored areas* depict the superior-temporal (*red*) and inferior-temporal (*blue*) regions.

location of the main temporal superior and inferior blood vessels correlated with the RNFL thickness profile. In a recent study, Yamashita et al.[14] reported that the retinal artery angle was highly correlated with the peak angle of the RNFL thickness. Given this close relationship between the retinal vasculature and the RNFL thickness profile in the peripapillary region, we hypothesize that the blood vessel pattern may be helpful to describe the RNFB trajectories.

The purpose of this study was to determine the relationship between the retinal vessel course and the variability of the RNFB trajectories as described by a mathematical model in the human retina.

METHODS

Patient Data and Data Acquisition

We used a previously collected dataset comprising 28 fundus pictures of the right eye of 28 subjects.[7] These pictures were selected from patients who underwent digitized fundus photography as part of regular ophthalmic care in the University Eye Hospital Oulu, Finland. To ensure good visibility, only subjects without diseases affecting the RNFL or its visibility were included. As a consequence, most patients were relatively young (mean age 28 years) diabetic patients without diabetic retinopathy. Approval for the data collection was obtained according to the guidelines of the Ethical Committee of the Northern Ostrobothnia Hospital District. All subjects provided written informed consent. The study followed the tenets of the Declaration of Helsinki.

Variability of the Retinal Nerve Fiber Bundle Trajectories

Twenty-four trajectories per fundus photograph were traced, one per half clock hour. Figure 1 shows an example of a traced photograph. The fitting process has been described before.[6,7] In short, the trajectories were fitted in a modified polar coordinate system (r,φ), with r representing the distance from the center of the optic nerve head (ONH) and φ the corresponding angle. In this coordinate system, the trajectories were described by:

$$\varphi(\varphi_0, r) = \varphi_0 + b(\varphi_0) \cdot (r - r_0)^{c(\varphi_0)} \quad (1)$$

where $\varphi_0 = \varphi(r = r_0)$ is the angular position of the trajectory at its starting point at a circle with radius r_0 around the center of the ONH, b a real number, and c a positive real number. Parameter c determines the location of the curvature (punctum maximum of curvature close to the disc for $c < 1$ and farther away from the disc for $c > 1$) while b determines the amount of curvature. The required nonlinear fitting was solved by performing a two-stage fitting process. In the first stage, the relationship between c and φ_0 was evaluated and substituted in Equation 1. The second stage of the fitting process yielded an ln b (superior half of the retina) or ln($-b$) (inferior half) value for each trajectory. The deviation of a trajectory from the previously published model was defined as the difference between the ln b or ln($-b$) value of the trajectory and the corresponding ln b or ln($-b$) value as predicted by the model.[6] The average difference within a region of interest was depicted by the variable "mean departure."[7] The mean departure was determined for each individual, for the superior-temporal (right eye clock hours 9 to 1) and the inferior-temporal (clock hours 5 to 9) region separately. The left column of Figure 2 shows, for the superior-temporal region, the original model (middle row) and the model $\pm$ 1 standard deviation of mean departure (upper and lower row, respectively). The right column of Figure 2 presents the corresponding data for the inferior-temporal region. See legend to Figure 2 for details. The standard deviation was 0.2 for both regions.

Blood Vessel Angles

The ImageJ software (available in the public domain at http://rsbweb.nih.gov/ij/; www.nih.gov, National Institutes of Health, Bethesda, MD, USA) was used in order to mathematically describe the retinal blood vessel courses. Firstly, a rectangle was fitted to the height and width of the ONH manually. Two diagonal lines were drawn, and their crossing was considered the ONH center. Three circles with radii equaling 25% (circle 1), 50% (circle 2), and 100% (circle 3) of the distance between the ONH center and the fovea were drawn around the ONH center. Figure 3 shows these circles. The intersections of the major temporal retinal blood vessels (superior artery, superior vein, inferior artery, and inferior vein) and the circles were determined. Subsequently, we measured the angles between a line through the ONH center and the fovea and the lines through the ONH center and the intersections. In this way, three series of four angles were defined: superior artery angle (SAAi), superior vein angle (SVAi), inferior artery angle (IAAi), and inferior vein angle (IVAi), where i is the circle number; Figure 3 shows the angles for i = 2. Additionally, we marked the arteriovenous crossing of the first order away from the ONH in the superior-temporal and inferior-temporal region. In this way, another two angles were defined: superior crossing angle (SCA) and inferior crossing angle (ICA). These angles reflect the position of the vascular arcades and are also shown in Figure 3. SAAi+IAAi and SVAi+IVAi correspond to the artery angle and vein angle, respectively, as used by Yamashita et al.[14] SCA+ICA corresponds to the angle between temporal vessel arcades as used by Fledelius and Goldschmidt.[15]

Refraction and Optic Disc Inclination

Refraction was recorded as the spherical equivalent refraction. The inclination of the ONH was quantified by the angle between a line through the ONH center and fovea and a horizontal line through the fovea.

Statistical Analysis

The superior-temporal and inferior-temporal region were analyzed separately. The associations between mean departure

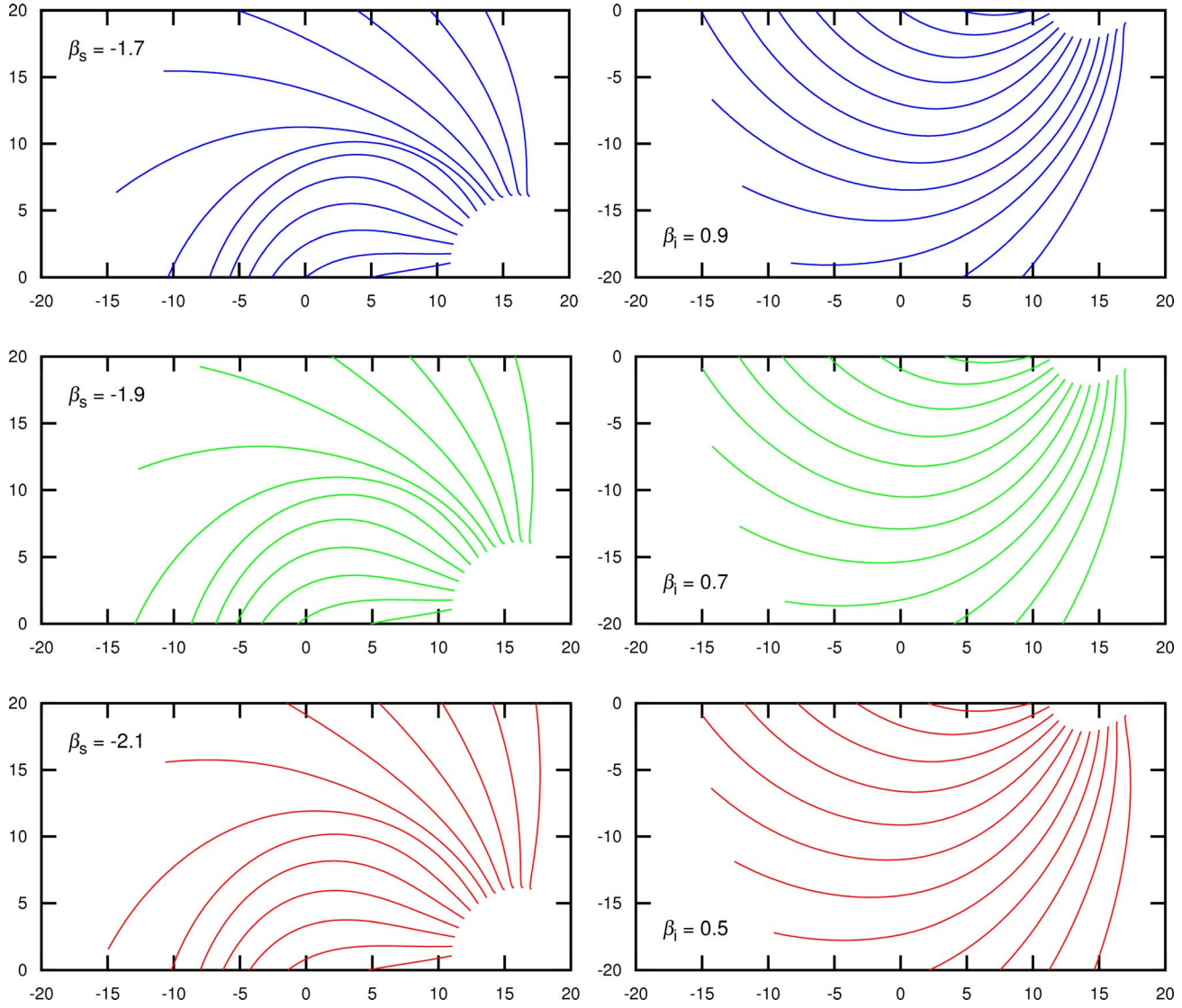

Figure 2. Original model (*middle row*) and model ± 1 standard deviation of mean departure (*upper and lower row*, respectively) for the superior-temporal (*left column*) and inferior-temporal (*right column*) region. The *x*- and *y*-axes depict position (eccentricity) in degrees. Parameters β_s and β_i belong to the mathematical model[6]; mean departure has to be added to the default values of these parameters (−1.9 for the superior-temporal region; 0.7 for the inferior-temporal region). See also the antepenultimate paragraph of the Discussion section.

on the one hand and blood vessel angles, refraction, and optic disc inclination on the other hand were analyzed with Pearson correlation analysis. Multiple linear regression analysis was used to determine the influence of refraction, optic disc inclination, and blood vessel angles on the mean departure. Initial multiple linear regression models were made for all three circles and for the crossing angle separately. Independent variables with $P > 0.05$ were subsequently removed, and the model with the highest adjusted R^2—one model for each region—was considered the final model. All analyses were performed using R (version 2.11.1 for Linux; R Foundation for Statistical Computing, Vienna, Austria). For multiple linear regression, the lm function of R was used.

Results

Table 1 shows the descriptive statistics of the involved variables. Table 2 presents the results of the corresponding correlation analysis. In the superior-temporal region, there was a significant association between mean departure and SAA1, SAA2, and refraction (i.e., spherical equivalent). In the inferior-temporal region, there was a significant association between mean departure and IAA3 and IVA2. Corresponding vessel angles from the superior and inferior hemifield were essentially not associated (all with $P > 0.07$), nor were the mean departure superior-temporal and the mean departure inferior-temporal ($r = 0.21$; $P = 0.27$).

Tables 3 and 4 present the initial (Table 3) and final (Table 4) multiple linear regression models. The most significant (highest adjusted R^2) models were those involving circle 2 for the superior-temporal region and circle 3 for the inferior-temporal region. The overall explained variance (R^2) was 0.54 for the superior-temporal region and 0.32 for the inferior-temporal region. If only the vessel angles were available, then the best model for the superior-temporal region is as follows: Mean departure = 0.0132*SAA2 − 0.969.

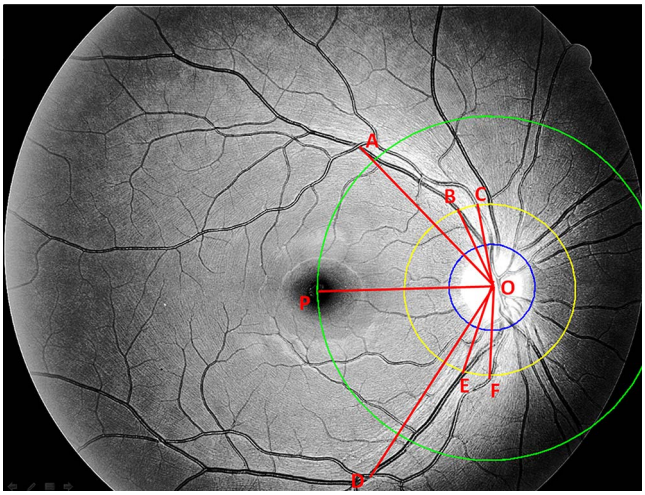

FIGURE 3. Blood vessel angles were defined at various distances from the optic nerve head (ONH) using the intersections of the major temporal retinal blood vessels (superior artery, superior vein, inferior artery, and inferior vein) and circles around the ONH center: superior arterial angle (SAA; C-P), superior venous angle (SVA; B-P), inferior arterial angle (IAA; F-P), and inferior venous angle (IVA; E-P). These angles were defined for circles with radii of 25% (circle 1; *blue*), 50% (circle 2; *yellow*; for this circle the angles are shown in the figure), and 100% (circle 3; *green*) of the ONH-to-fovea distance. Two more angles were defined using the arteriovenous crossing of the first order away from the ONH: superior crossing angle (SCA; A-P) and inferior crossing angle (ICA; D-P). Vertex at O for all angles.

DISCUSSION

In the superior-temporal region, refraction, ONH inclination, and SAA2 were the main determinants of the RNFB trajectories; in the inferior-temporal region, IAA3 was the main determinant. Clearly, the site where the vessel topography is assessed is important: The optimal site was closer to the ONH superiorly (circle 2) than it was inferiorly (circle 3), and the location of the vascular arcades, as depicted by the crossing angle, did not provide any useful information. Arteries were more informative than veins.

In our earlier studies, we demonstrated a significant interindividual variability of the RNFB trajectories and addressed the role of refraction and ONH inclination.[6,7] In the current study, both refraction and ONH inclination were significant in the multivariable analysis, at least in the superior-temporal region (Table 4). This implies that refraction is associated with the RNFL trajectories. For ONH inclination, the significance could either reflect a truly

TABLE 1. Characteristics of the Included Eyes, $n = 28$

	Median	IQR	Range
Mean departure superior-temporal	0.00	−0.11 to 0.18	−0.57 to 0.34
Mean departure inferior-temporal	0.09	−0.075 to 0.21	−0.36 to 0.41
Refraction, D	0.00	−1.25 to +1.13	−8.75 to +6.25
ONH inclination, °	4.8	3.7 to 6.9	0.8 to 10.6
SAA1, °	86.8	79.9 to 93.4	59.9 to 109.5
SVA1, °	86.2	78.8 to 94.8	54.2 to 110.5
IAA1, °	81.6	70.3 to 95.8	58.3 to 112.7
IVA1, °	82.8	70.7 to 97.8	52.1 to 104.2
SAA2, °	71.8	67.0 to 78.6	58.4 to 99.6
SVA2, °	72.2	66.5 to 79.2	56.7 to 94.0
IAA2, °	67.2	59.8 to 79.7	51.0 to 100.9
IVA2, °	67.8	60.5 to 80.7	49.8 to 93.6
SAA3, °	56.8	52.8 to 61.6	23.7 to 104.8
SVA3, °	59.1	55.3 to 64.5	28.7 to 92.9
IAA3, °	52.1	48.5 to 60.5	40.5 to 82.7
IVA3, °	52.8	45.1 to 60.9	41.6 to 76.0
SCA, °	56.2	48.3 to 59.9	36.0 to 69.7
ICA, °	50.1	39.8 to 56.2	26.7 to 73.0

IQR, interquartile range; D, diopter; SAAi (with i 1, 2, or 3), superior arterial angle measured at circle i (defined in Fig. 3); SVAi, superior venous angle measured at circle i; IAAi, inferior arterial angle measured at circle i; IVAi, inferior venous angle measured at circle i.

TABLE 2. Correlation Analysis Between the Mean Departure (Average Individual Deviation From the Model) and Refraction, ONH Inclination, and the Various Blood Vessel Angles

	Mean Departure Superior-Temporal		Mean Departure Inferior-Temporal	
	r	*P* Value	*r*	*P* Value
Refraction	0.41	0.03	0.26	0.12
ONH inclination	−0.25	0.21	0.09	0.64
SAA1	0.44	0.02		
SAA2	0.57	0.001		
SAA3	0.24	0.22		
SVA1	0.31	0.10		
SVA2	0.28	0.15		
SVA3	0.26	0.18		
IAA1			0.26	0.19
IAA2			0.37	0.06
IAA3			0.57	0.002
IVA1			0.22	0.27
IVA2			0.41	0.03
IVA3			0.23	0.25
SCA	−0.12	0.56		
ICA			0.27	0.17

SAAi (with i 1, 2, or 3), superior arterial angle measured at circle i (defined in Fig. 3); SVAi, superior venous angle measured at circle i; IAAi, inferior arterial angle measured at circle i; IVAi, inferior venous angle measured at circle i.

TABLE 3. R^2, Adjusted R^2, and Significant Independent Variables at $P < 0.05$ of the Initial Multiple Linear Regression Models as a Function of the Location at Which the Vessel Angles Were Measured for the Superior-Temporal and Inferior-Temporal Regions

	R^2	Adjusted R^2	Included Independent Variables*
Superior-temporal			
Circle 1	0.42	0.32	Refr, **Inc**, **SAA1**, SVA1
Circle 2	0.54	0.46	**Refr**, **Inc**, **SAA2**, SVA2
Circle 3	0.33	0.22	**Refr**, Inc, SAA3, SVA3
Crossing	0.26	0.17	**Refr**, Inc, SCA
Inferior-temporal			
Circle 1	0.16	0.01	Refr, Inc, IAA1, IVA1
Circle 2	0.35	0.24	Refr, Inc, **IAA2**, **IVA2**
Circle 3	0.39	0.28	Refr, Inc, **IAA3**, IVA3
Crossing	0.10	−0.02	Refr, Inc, ICA

* Bold indicates significant at $P < 0.05$.

Refr, refraction; Inc, optic nerve head inclination; SAAi (with i 1, 2, or 3), superior arterial angle measured at circle i (defined in Fig. 3); SVAi, superior venous angle measured at circle i; IAAi, inferior arterial angle measured at circle i; IVAi, inferior venous angle measured at circle i.

Table 4. Final Multiple Linear Regression Models for the Superior-Temporal and Inferior-Temporal Regions

	R^2	Adjusted R^2	Coefficient	Standard Error	*P* Value
Superior-temporal	0.54	0.49			
Intercept			−0.748		
Refraction, D			0.024	0.009	0.017
ONH inclination, °			−0.031	0.012	0.021
SAA2, °			0.012	0.003	<0.001
Inferior-temporal	0.32	0.29			
Intercept			−0.516		
IAA3			0.011	0.003	0.002

SAA2, superior arterial angle measured at circle 2 (defined in Fig. 3); IAA3, inferior arterial angle measured at circle 3.

independent effect or arise from the preprocessing of the fitting process (the ONH inclination influences the way a fundus picture is embedded in the modified polar coordinate system).[6] In both cases, adding information regarding ONH inclination to the model improves precision. For the current study it is important that the variability in ONH inclination is small compared to the variability in the vessel angles (Table 1). In the present study, the importance of the retinal blood vessel topography was uncovered. By adding information from the vessel topography, the explained variance increased from 0.28 and 0.08 (previous study)[7] to 0.54 and 0.32 (this study) for the superior-temporal and inferior-temporal region, respectively. As biological systems always show intrinsic variability, it is unlikely that much higher explained variances will be reached by adding more, currently unknown, determinants. Moreover, the tracing process itself also contributes to the variability.[16] For the dataset used in the current study, the interobserver variability was addressed earlier.[7] There was no bias between the two observers, and the interobserver variability was clearly smaller than the overall variability, albeit not negligible.

Our findings concerning the overall variability and the influence of refraction and ONH inclination on the RNFB trajectories agreed well with other studies[1,8,10] and have been discussed in detail before.[6,7] To the best of our knowledge, the significant influence of the retinal blood vessel topography on the RNFB trajectories has not been addressed before. However, an association between the retinal blood vessel positions and the peripapillary RNFL thickness profile has been reported, both with scanning laser polarimetry (at 3.2 mm from the ONH center)[13] and with optical coherence tomography (at 3.5 mm from the ONH center).[14,17] In these studies, the effect of the blood vessels on the RNFL thickness profile could have been, at least partially, an artifact due to a direct contribution of the blood vessels to the RNFL thickness profile measurement.[18] This is not the case in our study, due to a different methodology (traced trajectories versus thickness measurements).

Why are the retinal blood vessel topography and the RNFB trajectories associated? Blood vessels and nerves tend to develop in relative proximity, and the neuronal and vascular system may share common guidance signals during development.[11,12,19,20] The spindle cells, which become canalized later to form capillaries, invade the retina from the ONH and grow along the retinal ganglion cell layer/RNFL interface.[12,21] Because of the resulting close relationship between the neuronal and vascular system in the retina, one would expect to find a significant association between the retinal blood vessel topography and the RNFB trajectories all over the retina. However, the association seems to be limited to the vicinity of the ONH. In our study, the angles depicting the positions of the vascular arcades (SCA and ICA) were not associated with the RNFB trajectories. One possible explanation for this is the thick RNFL in the vicinity of the ONH, as opposed to the thin RNFL in areas that are farther away from the ONH.

In the present study, the superior and inferior hemifield were studied separately. Both the RNFB trajectories and the vessel angles were essentially uncorrelated between the two hemifields (see Results section). Moreover, an RNFB trajectory asymmetry between the two hemifields was found previously.[6,7] Joining the angles into artery angle (SAAi+IAAi) and vein angle (SVAi+IVAi), as described by Yamashita et al.,[14] did not yield significant associations, nor did combining SCA and ICA as used by Fledelius and Goldschmidt[15] (results not shown). This indicates that the neuronal and vascular system share an asymmetry between the superior and inferior hemifields in the human retina.

A limitation of our study is the sample size—the sample comprised 28 eyes of 28 subjects. We addressed this, to some extent, by limiting the number of independent variables in our multivariable analysis. A larger Caucasian dataset and especially a repeat in other ethnicities should precede the use of our findings in health care applications.

How can our results be applied to build personalized models? For a given individual, mean departure values can be calculated for both hemifields using Table 4. Subsequently, a personalized model can be plotted using the previously published equations[6] with the calculated mean departure values added to ln b or ln($-b$). This is illustrated in Figure 2. This approach assumes that, for a given individual, the differences between the ln b or ln($-b$) values of the traced trajectories and the corresponding values as predicted by the model are—within a region of interest—essentially independent of parameter φ_0 (the clock hour).[6] Although this was not formally tested, it has to be the case because otherwise trajectories would cross in some regions and would leave other regions unwired. Neither of these situations is observed in reality.

The explained variances of 0.54 and 0.32 are not self-evidently sufficiently high for an optimal assessment of glaucoma.[22] However, advances in optical coherence tomography (OCT) presumably allow for an individual measurement of the RNFB trajectories in the near future.[23] As the signal-to-noise ratio of such a measurement will be inherently limited, an underlying model that serves as a starting point will always be needed. Our model may serve as this starting point.

In conclusion, the retinal blood vessel topography explains a significant part of the distribution of the RNFL bundle trajectories in the human retina, but only if (1) the vessels are assessed at an appropriate distance from the ONH and (2) the superior and inferior hemifield are addressed independently. This should be taken into account in future individualized mathematical models describing the RNFB trajectories.

Acknowledgments

Presented at the annual Image meeting, Dresden, Germany, March 2014.

Supported by the University of Groningen Abel Tasman Talent Program (University Medical Center Groningen/Shantou University Medical College). The funding organizations had no role in the design, conduct, analysis, or publication of this research.

Disclosure: **K. Qiu**, None; **J. Schiefer**, None; **J. Nevalainen**, None; **U. Schiefer**, Pfizer (F), MSD (F), Haag-Streit (C), Pharm-Allergan (C); **N.M. Jansonius**, None

References

1. Garway-Heath DF, Poinoosawmy D, Fitzke FW, Hitchings RA. Mapping the visual field to the optic disc in normal tension glaucoma eyes. *Ophthalmology*. 2000;107:1809–1815.
2. Airaksinen PJ, Doro S, Veijola J. Conformal geometry of the retinal nerve fiber layer. *Proc Natl Acad Sci U S A*. 2008;105: 19690–19695.
3. Turpin A, Sampson GP, McKendrick AM. Combining ganglion cell topology and data of patients with glaucoma to determine a structure-function map. *Invest Ophthalmol Vis Sci*. 2009;50: 3249–3256.
4. Ferreras A, Pablo LE, Garway-Heath DF, Fogagnolo P, García-Feijoo J. Mapping standard automated perimetry to the peripapillary retinal nerve fiber layer in glaucoma. *Invest Ophthalmol Vis Sci*. 2008;49:3018–3025.
5. Kanamori A, Naka M, Nagai-Kusuhara A, Yamada Y, Nakamura M, Negi A. Regional relationship between retinal nerve fiber layer thickness and corresponding visual field sensitivity in glaucomatous eyes. *Arch Ophthalmol*. 2008;126:1500–1506.
6. Jansonius NM, Nevalainen J, Selig B, et al. A mathematical description of nerve fiber bundle trajectories and their variability in the human retina. *Vision Res*. 2009;49:2157–2163.
7. Jansonius NM, Schiefer J, Nevalainen J, Paetzold J, Schiefer U. A mathematical model for describing the retinal nerve fiber bundle trajectories in the human eye: average course, variability, and influence of refraction, optic disc size and optic disc position. *Exp Eye Res*. 2012;105:70–78.
8. Denniss J, McKendrick AM, Turpin A. An anatomically customizable computational model relating the visual field to the optic nerve head in individual eyes. *Invest Ophthalmol. Vis. Sci*. 2012;53:6981–6990.
9. Carreras FJ, Medina J, Ruiz-Lozano M, Carreras I, Castro JL. Virtual tissue engineering and optic pathways: plotting the course of the axons in the retinal nerve fiber layer. *Invest Ophthalmol Vis Sci*. 2014;55:3107–3119.
10. Lamparter J, Russell RA, Zhu H, et al. The influence of intersubject variability in ocular anatomical variables on the mapping of retinal locations to the retinal nerve fiber layer and optic nerve head. *Invest Ophthalmol Vis Sci*. 2013;54:6074–6082.
11. Carmeliet P, Tessier-Lavigne M. Common mechanisms of nerve and blood vessel wiring. *Nature*. 2005;436:193–200.
12. Provis JM. Development of the primate retinal vasculature. *Prog Retin Eye Res*. 2001;20:799–821.
13. Resch H, Brela B, Resch-Wolfslehner C, Vass C. Position of retinal blood vessels correlates with retinal nerve fibre layer thickness profiles as measured with GDx VCC and ECC. *Br J Ophthalmol*. 2011;95:680–684.
14. Yamashita T, Asaoka R, Tanaka M, et al. Relationship between position of peak retinal nerve fiber layer thickness and retinal arteries on sectoral retinal nerve fiber layer thickness. *Invest Ophthalmol Vis Sci*. 2013;54:5481–5488.
15. Fledelius HC, Goldschmidt E. Optic disc appearance and retinal temporal vessel arcade geometry in high myopia, as based on follow-up data over 38 years. *Acta Ophthalmol*. 2010;88:514–520.
16. Denniss J, Turpin A, Tanabe F, Matsumoto C, McKendrick AM. Structure–function mapping: variability and conviction in tracing retinal nerve fiber bundles and comparison to a computational model. *Invest Ophthalmol Vis Sci*. 2014;55: 728–736.
17. Pereira I, Weber S, Holzer S, et al. Correlation between retinal vessel density profile and circumpapillary RNFL thickness measured with Fourier-domain optical coherence tomography. *Br J Ophthalmol*. 2014;98:538–543.
18. Hood DC, Fortune B, Arthur SN, et al. Blood vessel contributions to retinal nerve fiber layer thickness profiles measured with optical coherence tomography. *J Glaucoma*. 2008;17:519–528.
19. Dorrell MI, Friedlander M. Mechanisms of endothelial cell guidance and vascular patterning in the developing mouse retina. *Prog Retin Eye Res*. 2006;25:277–295.
20. Eichmann A, Makinen T, Alitalo K. Neural guidance molecules regulate vascular remodeling and vessel navigation. *Genes Dev*. 2005;19:1013–1021.
21. Ashwell KW, Waite P. Development of the peripheral nervous system. In: Paxinos G, Mai JK, eds. *The Human Nervous System*. 2nd ed. Amsterdam: Elsevier Academic Press; 2004: 95–110.
22. Springelkamp H, Lee K, Wolfs RCW, et al. Population-based evaluation of retinal nerve fiber layer, retinal ganglion cell layer, and inner plexiform layer as a diagnostic tool for glaucoma. *Invest Ophthamol Vis Sci*. 2014;55:8428–8438.
23. Sugita M, Pircher M, Zotter S, et al. Retinal nerve fiber bundle tracing and analysis in human eye by polarization sensitive OCT. *Biomed Opt Express*. 2015;6:1030–1054.

Investigative Ophthalmology & Visual Science